EPJ Web of Conferences **293**, 00033 (2024) https://doi.org/10.1051/epjconf/202429300033
mm Universe 2023

Estimation of the hydrostatic-to-lensing mass bias from resolved cluster masses

M. Muñoz-Echeverría[1,*], J. F. Macías-Pérez[1], G. W. Pratt[2], E. Pointecouteau[3], I. Bartalucci[4], M. De Petris[5], A. Ferragamo[5,6], C. Hanser[1], F. Kéruzoré[7], F. Mayet[1], A. Moyer-Anin[1], A. Paliwal[5], L. Perotto[1], and G. Yepes[8,9]

[1]Univ. Grenoble Alpes, CNRS, LPSC-IN2P3, 53, avenue des Martyrs, 38000 Grenoble, France
[2]Université Paris-Saclay, Université Paris Cité, CEA, CNRS, AIM, 91191 Gif-sur-Yvette, France
[3]Univ. de Toulouse, UPS-OMP, CNRS, IRAP, 31028 Toulouse, France
[4]INAF, IASF-Milano, via A. Corti 12, I-20133 Milano, Italy
[5]Dipartimento di Fisica, Sapienza Università di Roma, Piazzale Aldo Moro 5, I-00185 Roma, Italy
[6]Instituto de Astrofísica de Canarias (IAC), C/Vía Láctea s/n, 38205 La Laguna, Tenerife, Spain
[7]High Energy Physics Division, Argonne National Laboratory, Lemont, IL 60439, USA
[8]Departamento de Física Teórica and CIAFF, Facultad de Ciencias, UAM, 28049 Madrid, Spain
[9]Centro de Investigación Avanzada en Física Fundamental (CIAFF), UAM, 28049 Madrid, Spain

Abstract. We present a study on the bias of hydrostatic masses with respect to lensing mass estimates for a sample of 53 clusters in a redshift range between $z = 0.05$ and 1.07. The M_{500} mass for each cluster was inferred from X-ray and lensing data, without using a priori observable-mass scaling relations. Cluster masses of our reference analysis were reconstructed homogeneously and we assess the systematic dispersion of those homogeneous masses with respect to other published mass estimates. We obtain an hydrostatic-to-lensing mass bias of $(1 - b) = 0.74^{+0.08}_{-0.07}$ and no significant evidence of evolution with redshift.

1 Introduction

The masses of clusters of galaxies are an essential ingredient for their use in cosmology [1–3]. In fact, the distribution of galaxy clusters in mass and redshift is sensitive to the expansion history and to the matter content of the Universe, as well as to the initial conditions in the primordial Universe [4]. Under the hydrostatic equilibrium (HSE) assumption, we can reconstruct the mass of individual clusters from the observation of their intracluster medium. Nevertheless, it has been extensively investigated and proved that masses reconstructed under this hypothesis are biased low [5–8]. The so-called *HSE mass bias* is defined as the relative difference of HSE mass estimates to the true cluster masses, $(1 - b) = M^{\rm HSE}/M^{\rm True}$. For the cluster number count cosmological analyses based on HSE masses, the HSE mass bias could be one of the possibilities to solve the current $\Omega_{\rm m} - \sigma_8$ tension between the cosmological results obtained from late-Universe large scale structures and CMB anisotropies [6, 9]. The real value of this bias, if any, has been largely debated in the literature [8], but to date, there is not a clear agreement. The potential evolution of the HSE mass bias with the redshift of clusters is not well understood either.

*e-mail: miren.munoz@lpsc.in2p3.fr

In this work we aim at comparing HSE masses to lensing mass estimates, and, thus, measuring the HSE-to-lensing mass bias as a proxy of the HSE bias, $(1-b) = M^{\rm HSE}/M^{\rm True} \sim M^{\rm HSE}/M^{\rm lens}$. A large number of methods and models can be employed to reconstruct cluster masses and these estimates could potentially be subject to different biases. Thus, we restrict the analysis to a sample of clusters for which X-ray based HSE and lensing masses have been reconstructed from direct mass estimations for each cluster individually. We build a sample of clusters that spans a large redshift range and select homogeneous (see Sect. 2.1) mass estimates. In addition, we propagate the systematic dispersion of the homogeneous masses, which goes one step beyond previous studies [10–12].

This proceeding is structured as follows: in Section 2 we describe the selection and characterisation of the analysed sample of clusters, Section 3 presents the measurement of the HSE-to-lensing mass bias and its evolution with redshift. The intrinsic scatter of HSE and lensing mass estimates are accounted for in Section 4, and conclusions are drawn in Section 5.

2 Sample selection

In this section we present the datasets that we have combined to build the sample of clusters used for the estimation of the HSE-to-lensing bias.

2.1 The datasets

Aiming to measure any potential redshift evolution of the bias, we have built a sample of clusters that covers the widest possible redshift range. At the same time, we select cluster HSE and lensing resolved masses that are comparable amongst all the objects in the sample (ensuring all masses are obtained through an *homogeneous* reconstruction procedure). Regarding the HSE masses, we make use of a compilation of clusters[1] with hydrostatic masses reconstructed following the method described in [13] based (mainly) on XMM-*Newton* data. For the lensing estimates, we consider the clusters from the Literature Catalogs of weak Lensing Clusters (LC^2) compilation presented in [14], hereafter CoMaLit, with weak lensing masses obtained from different works in the literature and standardised to the same cosmology and definitions. We match clusters in XMM-*Newton* and CoMaLit catalogues on the basis of their coordinates. Every matching entry is then verified by comparing the redshifts given in the different catalogues. As a result, we obtain a sample of 65 clusters with HSE and lensing masses that can be used to measure the HSE-to-lensing mass bias.

However, as shown in [11, 15], cluster mass estimates can vary up to $\sim 40\%$ across different studies. Being aware of the important differences that exist between the masses reconstructed by different works, we have collected results from several studies in the literature (see [16] for the detailed list of works) that have also reconstructed cluster masses based on mass profiles. We use those estimates to measure the systematic dispersion, $\sigma^2_{\rm sys}$, of the HSE and lensing masses from those various studies with respect to our XMM-*Newton* and CoMaLit estimates. For HSE masses $\sigma^2_{\rm sys}$ is $\sim 30\%$ larger than the typical statistical uncertainties, while for lensing masses $\sigma^2_{\rm sys}$ is ~ 4 times smaller. Nevertheless, we show in [16] that these values vary with the clusters and works that are used to measure $\sigma^2_{\rm sys}$.

2.2 The *reference* sample

We perform additional checks on the 65 clusters with *homogeneous* X-ray and lensing masses and discard: 3 clusters with abnormally large uncertainties, and 9 clusters for which the

[1] A combination of ESZ [17] and LoCuSS [18] clusters at low redshift, LPSZ [19] clusters at intermediate redshift and the high-redshift sample analysed in Bartalucci+2018 [13].

centres assumed for the mass reconstructions in the X-ray and lensing studies are too distant for a reliable comparison.

As a result, we get a *reference* sample with homogeneous HSE and lensing masses for 53 clusters. In Figure 1 we present a summary of the characteristics of this *reference* sample. The histograms show the number of clusters with respect to redshift, HSE mass and lensing mass, the median values being respectively 0.253, 6.309×10^{14} $M_\odot$, and 8.772×10^{14} $M_\odot$. The sample is dominated by low-redshift clusters. However, while very few works in the literature go above $z = 0.5$, 20% of the clusters in our sample have redshifts higher than 0.5.

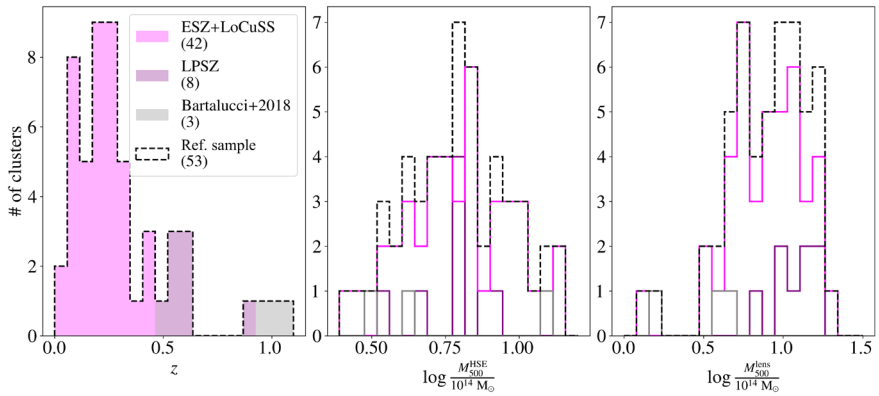

Figure 1. Redshift (left), HSE mass (centre) and lensing mass (right) distributions of the 53 clusters in the *reference* sample. The ESZ+LoCuSS, LPSZ and Bartalucci+2018 clusters are shown in magenta, purple and grey, respectively. The black dashed lines indicate the distributions for the full sample.

3 HSE-to-lensing mass bias

We describe the redshift evolution of the HSE-to-lensing mass bias following the parametrisation used in [20]:

$$M_{500}^{\rm HSE}/M_{500}^{\rm lens}(z) = (1-b)(z) = (1-\mathcal{B})\left(\frac{1+z}{1+z_*}\right)^{\beta_z}. \quad (1)$$

The redshift evolution is modelled by β_z, and $(1-\mathcal{B})$ corresponds to the bias normalised at the pivot redshift, z_*. Following [20], we consider the median redshift value of the clusters in the analysed sample as the pivot redshift.

The homogeneous HSE and lensing masses of the 53 clusters in the *reference* sample are used to perform a Markov chain Monte Carlo (MCMC) analysis to fit the model in Eq. 1 to data. Black markers in Figure 2 show the HSE-to-lensing mass ratio with respect to redshift for these 53 clusters. Error bars have been calculated from the quadratic sum of the measurement statistical uncertainties related to each cluster and the systematic scatter measured in Section 2. The grey shaded area in Figure 2 indicates the bias evolution model obtained from the posterior distributions of the fitted β_z and $(1-\mathcal{B})$ parameters. The horizontal dash-dotted, dotted and solid lines correspond respectively to the mean, median and error weighted mean HSE-to-lensing mass ratio obtained with the 53 cluster masses. Although there are hints of an evolution of the bias with redshift, we find that such trend is caused by the CL J1226.9+3332 cluster at $z = 0.89$. The dark grey area in Figure 2 shows the bias evolution model obtained by excluding the mentioned cluster from the sample.

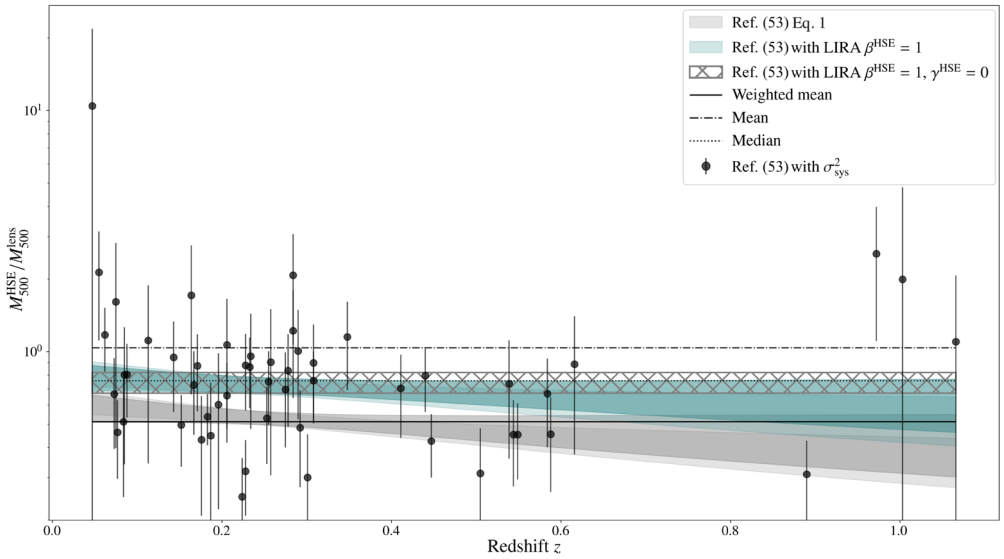

Figure 2. HSE-to-lensing mass ratio of the clusters in the *reference* sample with respect to redshift. Black data points show the mass ratio per cluster accounting for the systematic uncertainty. The error weighted mean, mean and median mass ratio for the data points are given by the horizontal solid, dash-dotted and dotted black lines, respectively. The grey shaded area indicates the evolution model of the bias (Eq. 1) when neglecting intrinsic scattters and accounting for all the clusters in the *reference* sample. In darker the result when excluding CL J1226.9+3332. The blue area corresponds to the evolution with redshift obtained from the fit of the scaling relation (SR) between HSE and lensing masses and the blue dark area is the evolution obtained for the *reference* sample excluding CL J1226.9+3332. The grey hatched area is the HSE-to-lensing mass ratio obtained from the fit of the SR when neglecting the redshift evolution.

4 HSE-to-lensing scaling relation

An alternative way for measuring the HSE-to-lensing mass bias, and accounting at the same time for the intrinsic scatter associated to HSE and lensing masses, is estimating the scaling relation (SR) between HSE and lensing masses [11]. We consider that both the HSE and the lensing masses are scattered and biased estimates of the true mass ($M^{\rm True}$) of clusters. Thus, we relate the masses such as

$$\ln M^{\rm lens} \pm \delta_{\rm lens} = \alpha^{\rm lens} + \beta^{\rm lens} \ln M^{\rm True} \pm \sigma^{\rm lens}, \tag{2}$$

and,

$$\ln M^{\rm HSE} \pm \delta_{\rm HSE} = \alpha^{\rm HSE} + \beta^{\rm HSE} \ln M^{\rm True} \pm \sigma^{\rm HSE} + \gamma^{\rm HSE} T. \tag{3}$$

Here all the masses in the arguments of logarithms are in 10^{14} $M_\odot$ units. The natural logarithm of the bias and the deviation from linearity are α and β, respectively, while $\sigma^{\rm lens}$ and $\sigma^{\rm HSE}$ correspond to the intrinsic scatter of the lensing and HSE masses with respect to the true mass. The measurement uncertainties associated with the logarithm of the lensing and HSE mass estimates for each cluster are given by $\delta_{\rm lens}$ and $\delta_{\rm HSE}$. Following [11], we fix $\alpha^{\rm lens} = 0$. A non-zero value of $\gamma^{\rm HSE}$ indicates redshift evolution and T is the time evolution factor, $T = \log\left(\frac{1+z}{1+z_{\rm ref}}\right)$, with $z_{\rm ref} = 0.01$ the normalisation redshift.

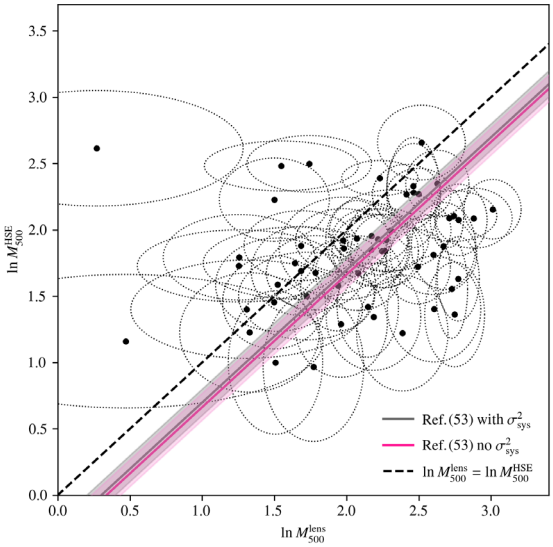

Figure 3. Scaling relation ($\gamma^{\rm HSE} = 0, \beta^{\rm HSE} = 1, \beta^{\rm lens} = 1$) between HSE and lensing masses in the *reference* sample. The masses in 10^{14} $M_\odot$ units of the 53 clusters in the sample are shown by the data points. Ellipses indicate the uncertainties in both axes accounting for the systematic scatter. The pink and grey lines correspond to the SR for the median value of parameters obtained without and with $\sigma_{\rm sys}$, respectively. Shaded regions show the 16th and 84th percentiles. The one-to-one relation is given by the black dashed line.

We perform the fit of the SR using the LInear Regression in Astronomy (LIRA) R package [21] and the `pylira`[2] Python wrapper. We consider different cases, by varying the parameters that are let free in the SR model. Given the large redshift range covered by our *reference* sample ($0.05 < z < 1.07$), it is particularly interesting to look for the evolution of the SR with redshift. Assuming that HSE and lensing masses scale linearly with the true mass ($\beta^{\rm lens} = \beta^{\rm HSE} = 1$), we obtain the bias evolution model shown in blue in Figure 2. Uniform priors were considered for the parameters: $\alpha^{\rm HSE} \sim \mathcal{U}(-4, 4)$, $\sigma^{\rm HSE} \sim \mathcal{U}(0, 10)$, $\sigma^{\rm lens} \sim \mathcal{U}(0, 10)$, and $\gamma^{\rm HSE} \sim \mathcal{U}(-10, 10)$. The comparison to the grey shaded area obtained in the previous section without accounting for the intrinsic scatter of HSE and lensing masses stresses upon the importance of considering such scatters in the bias estimation.

However, we verify that there is statistically no gain in adding the redshift evolution parameter $\gamma^{\rm HSE}$ to the SR model. In other words, redshift evolution does not seem to be favoured by the data. In conclusion, our best SR between X-ray HSE and lensing masses is given by the simplest scaling relation, with $\gamma^{\rm HSE} = 0$, $\beta^{\rm HSE} = 1$, and $\beta^{\rm lens} = 1$,

$$\ln M^{\rm lens} = \ln M^{\rm True} \pm 0.26^{+0.08}_{-0.09}, \tag{4}$$

$$\ln M^{\rm HSE} = -0.30^{+0.10}_{-0.10} + \ln M^{\rm True} \pm 0.17^{+0.09}_{-0.10}, \tag{5}$$

which corresponds to a HSE-to-lensing mass bias of $M^{\rm HSE}_{500}/M^{\rm lens}_{500} = (1 - b) = 0.74^{+0.08}_{-0.07}$ (stat. + sys.) $\pm$ 0.23 (intrin. scatter), where intrinsic scatters for lensing and HSE masses are assumed to be Gaussian.

Figure 3 shows this HSE-to-lensing mass SR obtained with the 53 clusters of the *reference* sample. Data points with ellipses correspond to each cluster in the sample. The ellipses account for the error bars in both axes when considering the systematic scatter (see Sect. 2), assuming no correlation between both mass estimates. The SR in grey has been obtained by accounting for the systematic scatter in the error bars of each cluster. By contrast, $\sigma^2_{\rm sys}$ was

[2]https://github.com/fkeruzore/pylira

not added to individual cluster uncertainties to obtain the scaling relation in pink. The black dashed line shows the one-to-one relation between X-ray HSE and lensing masses.

The hatched region in Figure 2 indicates the HSE-to-lensing mass bias resulting from this SR. Following [11] we have also cross-checked that this SR fits well different cluster subsamples in the *reference* sample, independently of the origin of the lensing mass estimates used to construct the CoMaLit catalogue.

5 Conclusions

This proceeding investigates the HSE-to-lensing mass bias with cluster masses inferred from resolved profiles. After a careful selection of clusters, we obtained a *reference* sample of 53 objects with redshifts spanning from $z = 0.05$ to 1.07. This constitutes the largest redshift range analysed homogeneously with this type of data for which we have access to X-ray HSE masses obtained from resolved profiles. Possible systematic effects in the *reference* analysis masses were taken into account by comparing the XMM-*Newton* and CoMaLit masses to other estimates from the literature. We propagated the derived systematic uncertainties to our analyses.

Accounting for the intrinsic scatter of HSE and lensing masses we obtain $(1 - b) = 0.74^{+0.08}_{-0.07}$ (stat. + sys.) ± 0.23 (intrin. scatter). We also find that ignoring the intrinsic scatters introduces a bias in the estimation of the HSE-to-lensing mass bias. Regarding the evolution of the HSE-to-lensing mass bias with redshift, we observe a trend towards a larger discrepancy between HSE and lensing masses at high redshift, but it is not statistically significant when excluding the CL J1226.9+3332 galaxy cluster from our sample. In conclusion, there is no evidence of evolution with redshift.

References

[1] A. Vikhlinin *et al.*, ApJ **692**, 1060 (2009)
[2] S. W. Allen, A. E. Evrard & A. B. Mantz, ARA&A **49**, 409 (2011)
[3] M. Costanzi *et al.*, MNRAS **488**, 4779 (2019)
[4] D. Huterer *et al.*, Astroparticle Physics **63**, 23 (2015)
[5] E. T. Lau, D. Nagai & K. Nelson, ApJ **777**, 151 (2013)
[6] Planck Collaboration XX., A&A **571**, A20 (2014)
[7] V. Biffi *et al.*, ApJ **827**, 112 (2016)
[8] G. Gianfagna *et al.*, MNRAS **502**, 5115 (2012)
[9] L. Salvati, M. Douspis & N. Aghanim, A&A **614**, A13 (2018)
[10] L. Lovisari *et al.*, A&A **644**, A78 (2020)
[11] M. Sereno & S. Ettori, MNRAS **450**, 3633 (2015)
[12] M. Sereno *et al.*, MNRAS **492**, 4528 (2019)
[13] I. Bartalucci *et al.*, A&A **617**, A64 (2018)
[14] M. Sereno, MNRAS **450**, 3665 (2015)
[15] M. Muñoz-Echeverría *et al.*, A&A **671**, A28 (2023)
[16] M. Muñoz-Echeverría *et al.*, A&A In press, arXiv:2312.01154
[17] Planck Collaboration XI., A&A **536**, A11 (2011)
[18] Planck Collaboration III., A&A **550**, A129 (2013)
[19] F. Mayet *et al.*, EPJ Web Conf. **228**, 00017 (2020)
[20] L. Salvati *et al.*, A&A **626**, A27 (2019)
[21] M. Sereno, MNRAS **455**, 2149 (2016)